UCRL-ID-121415

PCMDI
Program for Climate Model Diagnosis and Intercomparison

PCMDI Report No. 25

ESTIMATES OF ZONALLY AVERAGED TROPICAL DIABATIC HEATING IN AMIP GCM SIMULATIONS

by

James S. Boyle

Program for Climate Model Diagnosis and Intercomparison
Lawrence Livermore National Laboratory, Livermore, CA, USA

August 1995

PROGRAM FOR CLIMATE MODEL DIAGNOSIS AND INTERCOMPARISON
UNIVERSITY OF CALIFORNIA, LAWRENCE LIVERMORE NATIONAL LABORATORY
LIVERMORE, CA 94550

DISCLAIMER

Abstract

The vertical distribution of zonally and seasonally averaged diabatic heating is estimated for 29 GCM AMIP decadal simulations using the thermodynamic equation. Since only the zonally averaged, monthly means were available, the transient and stationary wave components are not included in this budget. The exclusion of these terms limits the useful analysis to the Tropics. The vertically averaged values from the budget computation are compared to the vertically averaged diabatic heating computed directly from the sensible heat and radiative fluxes, and precipitation. The comparison is quite favorable in the Tropics, with the effects of the neglected heat fluxes becoming apparent at about 30 degrees poleward from the Equator. The computations are carried out for the solstitial seasons.

Based on the median heating distribution of the 29 models we find the following. (1) The model consensus of near equatorial heating is greater in magnitude and lower (~500 mb) than that computed from the ECMWF analysis by Hoskins et al. (1989). (2) The sub-tropical cooling tends to be greater in magnitude and higher than the Hoskins et al. computation, although this will be affected by the terms neglected in the budget computation. Consideration of the individual model fields show that (3) there is a large variation in the magnitude and distribution of the tropical diabatic heating amongst the models. The magnitudes in the northern summer vary by more than a factor of two. (4) The amount of seasonal asymmetry about the equator varies widely among the models. For some models the heating maximum remains on the northern side of the equator for both seasons. (5) It is evident that the interactions among the many parameterizations and model formulations obscure any systematic signature of a particular penetrative convective scheme. Finally, given the differences in the heating distributions among the models for this zonally averaged, seasonally averaged ten year data set, it is clear that there is not yet a consensus on the proper parameterization suite to simulate this essential field.

1. Introduction

An understanding of the processess that generate the atmospheric diabatic heating rates is basic to an understanding of both the time averaged general circulation of the atmosphere and circulation anomalies. Knowledge of the sources and sinks of atmospheric heating enables a fuller understanding of the nature of the atmospheric circulation. An actual assesment of the diabatic heating rates in the atmosphere is a difficult problem that has been approached in a number of ways. One way is to estimate the total diabatic heating by estimating individual components associated with the radiative fluxes , the latent heat release, and sensible heat fluxes . An example of this approach is provided by Newell et al. (1974). Another approach is to estimate the net heating rates from consideration of the balance required of the mass and wind variables as routinely observed and analyzed. This budget computation has been done using the thermodynamic equation,e.g. Hoskins et. al. (1989) and more recently done by using the vorticity and thermodynamic equations, Sardeshmukh(1993). Schaak and Johnson (1991) compute the heating rates through the integration of the isentropic mass continuity equation. The estimates of heating arrived at all these methods are severely handicapped by the uncertainties in the observational data and analyses. In addition the estimates of the individual heating components suffer an additional source of error from the parameterizations used to approximate these quantities.

Figure 1 is taken from Hoskins et al. (1989) and shows the six year mean zonally averaged diabatic heating rate for the solsticial seasons. The data are the result of a residual calculation using ECMWF analyses in the thermodynamic equation. As Hoskins et al. (1989), Sardeshmukh (1993), and Trenberth and Olsen (1990) point out the ECMWF analyses are not without problems. Nevertheless, Figure 1 does represent an estimate of the zonally averaged diabatic heating which can be used as a basis for discussion.

The composition of the zonally averaged diabatic heating fields have been discussed by Grotjahn (1993), Newell et al. (1974) and numerous others. An overview is sketched here for interpreting some the the findings for the GCMs. Diabatic heating has three chief sources in the atmosphere, radiation, latent heat release, and sensible heat transfer from the surface. The radiational cooling is significant at the tropopause and is maximum at high latitudes. The cooling takes place off the tops of clouds. There

is some evidence of radiational warming in the equatorial stratosphere. The radiational cooling extends below the middle troposphere in the subtropics. Latent heat release is is found mainly in the Equatorial Tropics and secondarily in the midlatitude storm tracks. Sensible heating in the boundary layer is important in the subtropics and in the regions over the oceanic western boundary currents. The patterns of heating in Fig. 1 are consistent with a strong Hadley circulation and secondary Ferrel circulations and the seasonal shift of these features following the sun. It would be reasonable to expect the models to produce a heating pattern similar to Fig. 1. The effects of the transient eddy heat fluxes are to provide an effective heating in the high ans low troposphere in the subtropics and cooling at high latitudes at similar levels. They make a significant contribution to the total heating in the subtropics ans extratropics but their impact decreases rapidly in the Tropics.

The work of Sardeshmukh (1993) would indicate that the ECMWF values tend to be underestimates in general, with other localized deficiencies. One cannot expect an exact match from any model due to vageries in the data and interannual variations in the fields. For example the plots analogous to Fig. 1 from Schaack and Johnson (1991) indicate that the cooling in the subtropics does not have the lower level maxima near 600 mb seen in Fig. 1. The other features of Fig. 1 are consistent. The Schaack and Johnson result is only for the FGGE year using ECMWF level IIIb analyses. Newell et al. (1974) also present solstitial zonally averaged net heating rates. These do have significant differences from Fig. 1. There is a documented discrepancy in the calculation of the radiative heating, Dopplick (1979), used by Newell et al. this error makes exacting comparison unfruitful.

The focus here will be on estimates of the zonally averaged diabatic heating rates of GCMs in the Tropics. Because of data limitations, the requisite calculations cannot be made for the extratropics.The next section will present the details of the computations carried out to estimate the diabatic heating rates. The following section will describe the used in the analysis and some abbreviated characterizations of the models involved. The results for the models will then be summarized and some intercomparison will be examined.

2. Description of analysis

The zonally averaged, time mean diabatic heating can be calculated from the themodynamic equation as given by:

$$\overline{\frac{\partial}{\partial t}[T]} = \frac{\overline{Q}}{C_p} + \Gamma[\varpi] - \frac{[v]}{a}\frac{\partial}{\partial \varphi}\overline{[T]}$$

$$-\frac{1}{a\cos\varphi}\frac{\partial}{\partial \varphi}\left(\left[\overline{v^*T^*}\right] + \left[\overline{v'T'}\right]\right)\cos\varphi$$

$$-\frac{\partial}{\partial p}\left[\varpi^*T^* + \overline{\omega'T'}\right] + \frac{R}{C_p p}\left[\varpi^*T^* + \overline{\omega'T'}\right] \qquad (1)$$

where:

$$\Gamma \equiv \overline{[T]}\frac{\partial}{\partial p}\ln[\bar{\vartheta}] \quad \text{and } \vartheta = \text{potential temperature}.$$

where the overbars represent time averages, the brackets represent zonal means and the primes and asterisks represent the time and zonal deviations, respectively. All the other variables have their usual meteorolgical meanings.

The vertically integrated diabatic heating can be calculated from:

$$Q_{Total} = (\text{Net Radiation})_{TOA} + (\text{Net Radiation})_{Surface} \qquad (2)$$
$$+ (\text{Surface Sensible Heat Flux}) + (L * \text{precipitation})$$

where: Q_{TOT} is the total diabatic heating due to the sum of radiational, latent heat, sensible and frictional heating, TOA refers to the top of the atmosphere and L is the latent heat of evaporation. With the exception of the frictional component, all these

terms can be calculated directly from the data provided by the modeling groups in AMIP.

The data used in (1) are zonally averaged, monthly averaged winds and temperature fields at pressure levels. The data that are currently available for the AMIP integrations do not contain the transient and eddy components indicated in the last four terms of (1). Thus the estimates presented here are computed without these terms. It should be recognized that the interpolation of the model data to pressure surface will introduce imbalances in the budgets. In addition, there are errors due to estimates of the gradients due to horizontal and vertical discretization. All these computational errors will be added to the error due to omission of the eddy terms. In the Tropics, which will be of neccessity the focus of the discussion, the eddy terms are generally small. The data available do permit a gross check of the contribution of the eddy and transient terms in that the data are sufficient to compute the vertically integrated diabatic heating via (2) and this can be compared to the vertical integrated result of (1). In regions where the eddy terms are negligible and the errors in computing the terms are not overwhelming the two results should agree.

3. Data

The participants in AMIP simulate the global atmosphere for the decade 1979 to 1988 using a common solar constant, and CO2 concentration, and a common monthly averaged SST. and sea ice data set. An overview of AMIP is provided by Gates (1992).

The AMIP models used in this study are identified in Table 1 and their horizontal and vertical resolutions are shown. As important as the spatial configuration of the model are the parameterizations used to simulate moist convective heating, fluxes of heat, moisture and momentum, precipitation, clouds and so forth. The complete specifications of the parameterizations used in the models are described in Philips (1994). The various penetrative convective parameterizations are probably crucial elements in the simulations for the regions discussed here but it is difficult to succinctly characterize them. For a specific scheme, say the Kuo scheme, there are so many variations and critical differences in implementations that identifying a parameterization by the single nomenclature can be misleading.

Radiational schemes can also differ radically from one implementation to another. For example, seemingly minor changes in the specification of clouds can have

profound impacts on the cooling rates generated by any particular scheme.

The AMIP standard archival data were monthly means with two spatial formats. One set consisted of global gridded data at the surface, 850 and 200 hPa, and top of atmosphere. The other set contained only zonally averaged data from pole to pole but with a vertical resolution comparable to the standard WMO reporting levels. The globally gridded data was used in (2), and the zonally averaged data in (1).

4. Results

Documenting the results from all the models corresponds to a great many figures. The bulk of these have been put in the Appendix. Selected figures will be drawn out into the main text for discussion. Figures A1 to A16 display pressure- latitude sections of diabatic heating estimates from (1) and curves of the zonally and vertically averaged estimates of diabatic heating from (1) and (2) for solstical seasons. The appendix figures show that in general the two vertically integrated heating rates estimates agree fairly well in the Tropics from 20S to 20N, with increasing differences poleward of these limits. The better agreement near the Equator would indicate that this poleward difference is due to the eddy terms and not just computational error. There is a systematic tendency for all the vertically integrated budget results to overestimate the cooling as 30N, S is approached. This is consistent with the observational evidence that the eddy fluxes contribute warming at the upper levels at these latitudes, for example Grotjahn(1993). The agreement between the two independent calculations is sufficent to give some credence to the vertical distribution of the heating.

Figures 2 and 3 display the median values and absolute deviations for all the model diabatic heating estimates computed using (1). If one peruses all the individual model plots in the Appendix, it can be seen that Fig. 2 does a fairly good job in capturing the most prominent common characteristics of the models' heating.The model median heating rates, Fig. 2, display two prominent differences with Fig. 1. First, the level of the maxima in the heating on the summer side of the Equator is substantially lower (~ 500 mb) in the models than in Fig. 1,(~300 mb). Second, Fig. 1 has well defined cooling maxima in the winter side of the Equator around 600 mb which are not evident in the model fields. These lower level maxima are not evident in the analysis of Schaack and Johnson (1991) for the FGGE year data although their results

are similar to Fig. 1 in most other respects. Overall the extrema of Fig. 2 are somewhat larger than Fig. 1. This not neccessarily a deficiency of the models. Sardeshmukh (1993) indicates that his seasonal mean estimates of the vertically averaged diabatic heating can be as much as a factor of three different from those of the Hoskins et al. (1989) in some regions.

The mean absolute deviations shown in Fig. 3 provide an estimate of the amount of disagreement among the models, which is a useful counterpoint to the consensus view of Fig. 2. The data for JJA, Fig. 3a, indicate that there is a maximum of variation along the maximum in the summer hemisphere. This indicates that there is some disagreement on the distribution and magnitude of the heating. The disagreement is not small, the deviation is about one third the values of the median at 10N. The other maximum in Fig. 3a at 10S, is indicative of even more serious discrepancies. In this region (~700 mb) the mean deviation is at least 0.25 C/day which is equal to and exceeds the values of the median. This is an uncertainty of the model consensus of about 100% in these latitudes. The DJF mean absolute deviations are displayed in Fig. 3b. There is a region of deviation maxima at 10N, in this region the median values are small and near zero. This indicates disagreement as to the sign of the heating. In the summer hemisphere maximum latitudes (~10S), the mean deviations are about a quarter of the values of the median. In the DJF data some models tend to produce two heating maxima, one near the equator and one farther in the summer hemisphere. The relatively broad maximum in Fig. 3b, is at least in part due to this splitting.

In both seasons there is considerable variations about the maxima of heating in the summer hemisphere but in terms of percentage the winter hemisphere approaches 100% disagreement in the mean for the maxima regions.This is probably in part related to the lack of consensus on the interseasonal movement of the heating maximum found near the Equator.

a. Some individual model comparisons

Comparing the median of Fig. 2 with all the individual plots in the Appendix, the variation amongst the models is rather striking. Nevertheless, Fig. 2 provides a fair estimate of the distribution of the heating with the chief variations being in the magnitude as opposed to position, especially in the Northern summer. For example,the values of the NMC model for are roughly in line with the observations in Fig. 1 while the NCA data are a factor of three larger.

The MPI and ECM WF models share a close common heritage, use the same res-

olution, and both use the identical penetrative convective scheme. There is an obvious strong similarity in the diabatic heating integrals and profiles (see Appendix figures). The CSU and UCLA models also have common origins, the same grid resolution and share the same type of convective parameterization. These two also show some similarity. The NRL model uses an Arakawa-Schubert scheme as does UCLA and CSU but it appears to be different. The NRL has a formulation substantially different from the CSU and UCLA models. This example invites caution against any simple categorization of the models on the basis of a few characteristics or parameterizations. Another interesting pair is the ECMWF and UGAMP models. These are similar in almost all respects, the only substantive difference being the penetrative convective schemes used. The UGAMP model uses the Betts-Miller scheme while the ECMWF uses the Tiedke mass flux formulation. Comparing the heating profiles from these two models, there can be seen distinct differences.

b. Comparison by penetative convective parameterization

A common aspect of the simulation data is a definite maximum at low levels near 10N and a upper level maximum or maxima on the southern side of the equator. One might speculate that the lower level maxima near 10N which varies from about 700 hPa to 850 hPa is due to shallow convection, while the deeper, higher level maximum is due to penetrative convection in the summer ITCZ. Given this premise it would perhaps be logical to see if any pattern emerges from considering the various convective parameterization schemes used in the models.

Table 2 gives a summary and convective and schemes used in the models. From the Table is is possible to pick out broad categories of penetrative convective schemes, such as moist convective adjustment (MCA), Arakawa-Schubert (A-S), Kuo (KUO) and mass flux (MFLX). The actual implementation of the details of the various schemes can vary widely and such simple categorizations are not without substantial ambiguity. The comparison problem is further compounded by differences in vertical and horizontal resolution.

Despite the problems, statistics were computed from selected subsets of the models, each subset consisting of models with nominally the same penetrative convective parameterization. Figure 4 displays the differences of the medians of these subsets from the grand median of all the models from Figure 2. The MCA group, Fig. 4a,b, tends to have more heating along the equator and less poleward than the median. The KUO group, Fig. 4cd, appears to underestimate the heating/cooling with extrema

about in the same positions as the grand values. The AS group, Fig. 4ef, has less well defined patterns. The MFLX models, Fig. 4gh, tend to over estimate the heating/cooling with respect to the median. However, Fig. 5 displays the mean absolute deviation for these subsets of models. It is obvious that the models with similar convective schemes can have very different heating in the Tropics, the differences being on the order seen in Fig. 3 for all the models. Thus, the convective parameterization is just a part of the picture and evidently does not necessarily play a dominant role in determining the character of the diabatic heating.

5. Conclusions

The vertical distribution of zonally and seasonally averaged diabatic heating is estimated for 29 GCM AMIP decadal simulations using the thermodynamic equation. Since only the zonally averaged, monthly means were available, the transient and stationary wave components are not included in this budget. The exclusion of these terms limits the useful analysis to the Tropics. The vertically averaged values from the budget computation are compared to the vertically averaged diabatic heating computed directly from the sensible heat and radiative fluxes, and precipitation. The comparison is quite favorable in the Tropics, with the effects of the neglected heat fluxes becoming apparent at about 30 degrees poleward from the Equator. The computations are carried out for the solstitial seasons.

Based on the median heating distribution of the 29 models we find that (1) The model consensus of near equatorial heating is greater in magnitude and lower (~500 mb) than that computed from the ECMWF analysis by Hoskins et al. (1989). (2) The sub-tropical cooling tends to be greater in magnitude and higher than the Hoskins et al. computation, although this will be affected by the terms neglected in the budget computation. Consideration of the individual model fields show that (3) there is a large variation in the magnitude and distribution of the tropical diabatic heating amongst the models. The magnitudes in the northern summer vary by more than a factor of two. (4) The amount of seasonal asymmetry about the equator varies widely among the models. For some models the heating maximum remains on the northern side of the equator for both seasons. (5) It is evident that the interactions among the many parameterizations and model formulations obscure any systematic signature of a particular penetrative convective scheme. Finally, given the differences in the

heating distributions among the models for this zonally averaged, seasonally averaged ten year data set, it is clear that there is not yet a consensus on the proper parameterization suite to simulate this essential field.

Acknowledgments. The generosity of the modeling groups involved in AMIP in making their results available is greatly appreciated. I also wish to acknowledge the useful comments of B. Dugas and M. Blackburn on a earlier version of the manuscript. This work was performed under the auspices of the Department of Energy Environmental Sciences Division by the Lawrence Livermore National Laboratory under contract W-7405-ENG-48.

6. References

Dopplick, T. G., 1979: Radiative heating of the global atmosphere: Corrigendum. *J. Atmos. Sci.*, **36**, 1812-1817.

Grotjahn, R., 1993: *Global atmospheric Circulations-Observations and Theories.*, Oxford University Press, New York, 430pp.

Hoskins, B. J., H. H. Hsu, I. N. James, M. Masutani, P. D. Sardeshmukh and G. H. White 1989: *Diagnostics of the global atmospheric circulation based on ECMWF analyses 1979-1989.* WCRP Report No. 27, WMO/TD No. 326, World Meteorological Organization, Geneva 217pp.

Newell, R. E., J. W. Kidson, D. G. Vincent, and G. J. Boer 1974: *The General circulation of the Tropical Atmosphere,* Volume 2. MIT Press, Cambridge, MA 371pp.

Phillips, T. J., 1994: *A Summary documentation of the AMIP models.* PCMDI report No. 18, University of California, Lawrence Livermore National Laboratory, Livermore CA 343pp.

Sardeshmukh, P. D., 1993: The baroclinic chi problem and its application to the diagnosis of atmospheric heating rates., *J. Atmos. Sci.*, **50**, 1099-1112.

Schack T. K., and D. R. Johnson, 1991: *Atlas of the Global Distribution of Atmospheric Heating during the Global Weather Experiment.*, NASA contractor Report No. 4370., National Aeronautics and Space administration, Washington D. C., 148pp.

Trenberth, K. E., and J. G. Olsen, 1988: *Evaluation of NMC Global Analyses: 1979-1987.* NCAR/TN-299+STR, Climate and Global Dynamics Division, National Center for Atmospheric Research, Boulder CO, 82 pp.

Trenberth, K. E., and J. G. Olsen, 1988: *Intercomparison of NMC and ECMWF Global Analyses: 1980-1986.* NCAR/TN-301+STR, Climate and Global Dynamics Division, National Center for Atmospheric Research, Boulder CO, 81 pp.

Table 1 : Model representation/resolution. The table lists the horizontal representation and resolution; vertical coordinates and number of prognostic vertical levels (number below 800 hPa, above 200 hPa); and atmospheric bottom and top pressure levels, for a surface pressure of 1000 hPa. Taken from Phillips (1994).

AMIP Model	Horizontal		Vertical		
	Representation	Resolution	Coordinates	No. Levels	Bottom, Top
BMRC	spectral	rhomboidal 31	sigma	9 (3, 3)	991, 9 hPa
CCC	spectral	triangular 32	hybrid	10 (3, 4)	980, 5 hPa
CNRM	spectral	triangular 42	hybrid	30 (4, 20)	995, 0.01 hPa
COLA	spectral	rhomboidal 40	sigma	18 (5, 4)	995, 10 hPa
CSIRO	spectral	rhomboidal 21	sigma	9 (3, 3)	979, 21 hPa
CSU	finite difference	4 x 5 degrees	modified sigma	17 (2, 6)	variable, 51 hPa
DERF	spectral	triangular 42	sigma	18 (5, 5)	998, 2 hPa
DNM	finite difference	4 x 5 degrees	sigma	7 (1, 1)	929, 71 hPa
ECMWF	spectral	triangular 42	hybrid	19 (5, 7)	996, 10 hPa
GFDL	spectral	rhomboidal 30	sigma	14 (4, 4)	997, 15 hPa
GISS	finite difference	4 x 5 degrees	sigma	9 (2, 2)	975, 10 hPa
GLA	finite difference	4 x 5 degrees	sigma	17 (5, 4)	994, 12 hPa
GSFC	finite difference	4 x 5 degrees	sigma	20 (5, 7)	994, 10 hPa
IAP	finite difference	4 x 5 degrees	modified sigma	2 (0, 0)	800, 200 hPa
JMA	spectral	triangular 42	hybrid	21 (6, 7)	995, 10 hPa
LMD	finite difference	50 sinlat x 64 lon	sigma	11 (3, 2)	979, 4 hPa
MGO	spectral	triangular 30	sigma	14 (5, 4)	992, 13 hPa
MPI	spectral	triangular 42	hybrid	19 (5, 7)	996, 10 hPa
MRI	finite difference	4 x 5 degrees	hybrid	15 (1, 9)	variable, 1 hPa
NCAR	spectral	triangular 42	hybrid	18 (4, 7)	992, 3 hPa
NMC	spectral	triangular 40	sigma	18 (5, 4)	995, 21 hPa
NRL	spectral	triangular 47	hybrid	18 (5, 5)	995, 1 hPa
RPN	spectral semi-Lagrangian	triangular 63	sigma	23 (7, 7)	1000, 10 hPa
SUNYA	spectral	rhomboidal 15	sigma	12 (3, 5)	991, 9 hPa
SUNYA/NCAR	spectral	triangular 31	hybrid/sigma	18 (4, 7)	993, 5 hPa
UCLA	spectral	4 x 5 degrees	modified sigma	15 (2, 9)	variable, 1 hPa
UGAMP	spectral	triangular 42	hybrid	19 (5, 7)	996, 10 hPa
UIUC	finite difference	4 x 5 degrees	sigma	7 (3, 0)	990, 200 hPa
UKMO	finite difference	2.5 x 3.75 degrees	hybrid	19 (4, 7)	997, 5 hPa
YONU	finite difference	4 x 5 degrees	modified sigma	5 (1, 1)	900, 100 hPa

Table 2 : Convection. The table lists references on schemes used for simulation of deep and shallow convection, with brief descriptions. Taken from Phillips (1994).

AMIP Model	Convection References	Descriptions
BMRC	Kuo (1974), Anthes (1977), Tiedtke (1988)	moisture convergence closure with shallow convection
CCC	Boer et al. (1984a)	moist convective adjustment
CNRM	Bougeault (1985), Geleyn (1987)	bulk mass flux scheme with shallow convection
COLA	Kuo (1965), Sela (1980), Tiedtke (1983)	moisture convergence closure with shallow convection
CSIRO	Arakawa (1972), Geleyn (1987)	relaxed moist adjustment with shallow convection
CSU	Arakawa & Schubert (1974)	interactive cumulus subensembles
DERF	Manabe et al. (1965), Tiedtke (1983)	moist convective adjustment with shallow convection
DNM	Kuo (1974), Anthes (1977)	moisture convergence closure with moist adjustment
ECMWF	Tiedtke (1989), Tiedtke et al. (1988)	bulk mass flux scheme with shallow convection
GFDL	Manabe et al. (1965)	moist convective adjustment
GISS	Del Genio & Yao (1988), Yao & Del Genio (1989)	convective plume with entrainment and downdrafts
GLA	Sud et al. (1991) modifications of Arakawa & Schubert (1974)	interactive cumulus subensembles with constraints on critical work function and minimum entrainment rate
GSFC	Moorthi & Suarez (1992)	relaxed solution of interactive cumulus subensembles
IAP	Arakawa et al. (1969), Zeng et al. (1989)	steady-state cumulus ensemble
JMA	modified Kuo (1974), Tiedtke (1983)	moisture convergence closure with shallow convection
LMD	Kuo (1965), Manabe & Strickler (1964)	moisture convergence closure with moist adjustment
MGO	Kuo (1974), Meleshko et al. (1991)	moisture convergence closure with moist adjustment
MPI	Tiedtke (1989), Tiedtke et al. (1988)	bulk mass flux scheme with shallow convection
MRI	Arakawa & Schubert (1974), Tokioka et al. (1988)	interactive cumulus subensembles with constraints on minimum entrainment rate
NCAR	Hack (1993)	mass flux scheme applied successively in three layers
NMC	Kuo (1965), Sela (1980), Tiedtke (1983)	moisture convergence closure with shallow convection
NRL	modified Arakawa & Schubert (1974), Tiedtke (1983)	interactive cumulus subensembles with downdrafts and shallow convection
RPN	Kuo (1974), Anthes (1977)	moisture convergence closure with shallow convection by generalized boundary-layer turbulence formulation
SUNYA	Manabe et al. (1965)	moist convective adjustment
SUNYA/NCAR	simplified Kreitzberg & Perkey (1976)	dry and moist sub-gridscale convective plume model
UCLA	Arakawa & Schubert (1974)	interactive cumulus subensembles
UGAMP	Betts & Miller (1994)	relaxed convective adjustment to reference profiles
UIUC	Arakawa & Schubert (1974)	interactive cumulus subensembles
UKMO	Gregory & Rowntree (1990)	bulk mass flux scheme with updrafts/downdrafts
YONU	Arakawa & Schubert (1974)	interactive cumulus subensembles

Table 3: Models used in comparing convective parameterizations.

Moist convective adjustment	Kuo	Arakawa-Schubert	Mass flux	Betts-Miller
CCC	BMRC	CSU	CNRM	UGAMP
CSIRO	COLA	GLA	ECMWF	
DERF	JMA	GSFC	MPI	
GFDL	MGO	MRI	NCAR	
SUNYA	NMC	NRL	UKMO	
	RPN	UCLA		

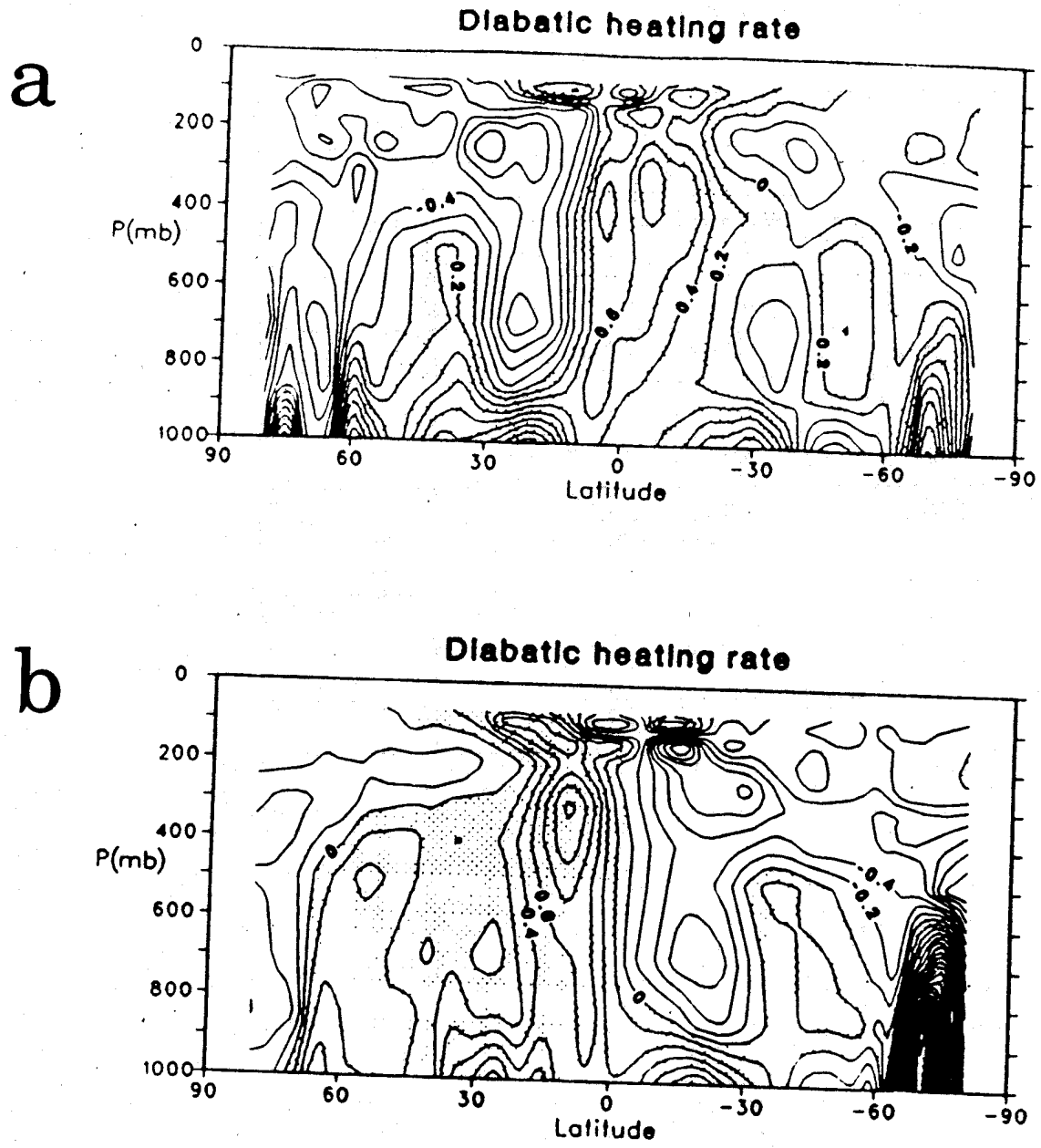

Figure 1. Six year average diabatic heating rate for (a) December through February and (b) June through August. Diabatic heating computed as a residual in the thermodynamic equation using the ECMWF operational analyses from 1983 to 1989. from Hoskins et al. (1989).

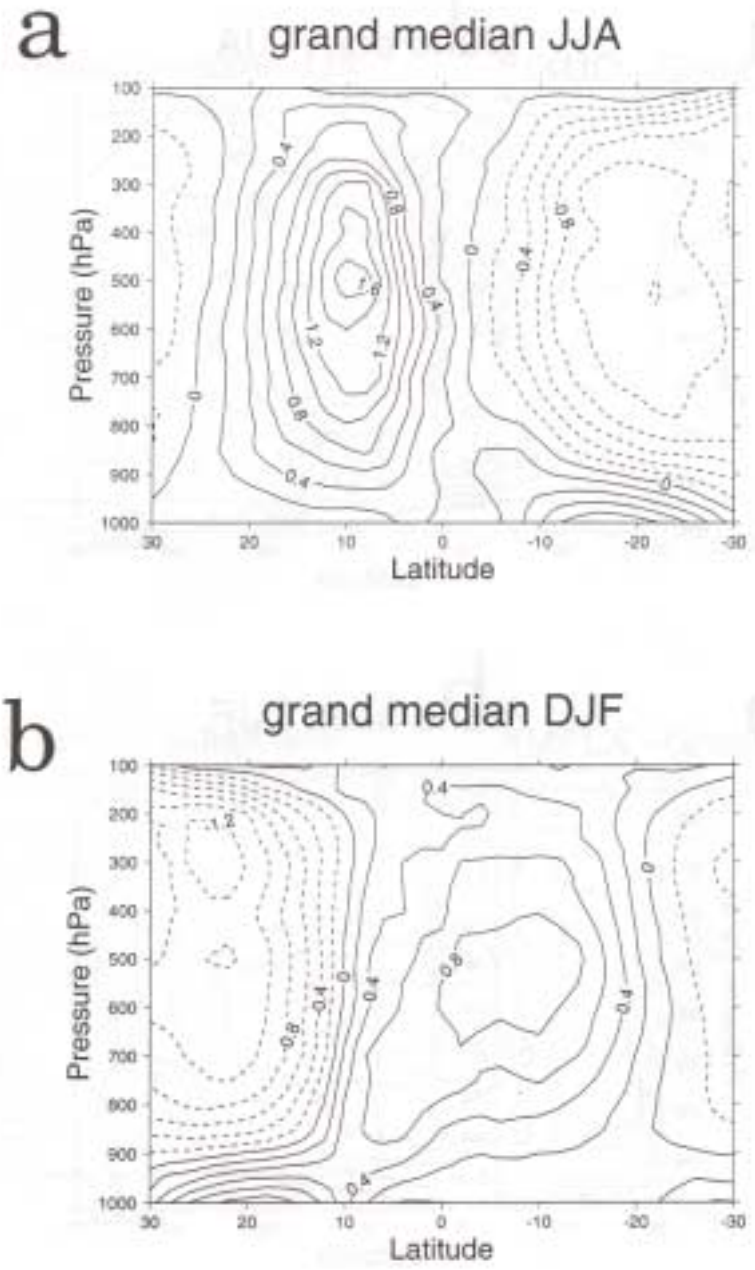

Figure 2. (a) The 29 model median diabatic heating rate for the Northern summer JJA computed using the technique described in the text. The domain extends from 30N to 30S. the negative values on the abcissa refer to southern latitudes. Contour interval is 0.2 deg C per day. Dash contours indicate negative values, solid contours are zero and above
(b) As in (a) except for the season DJF.

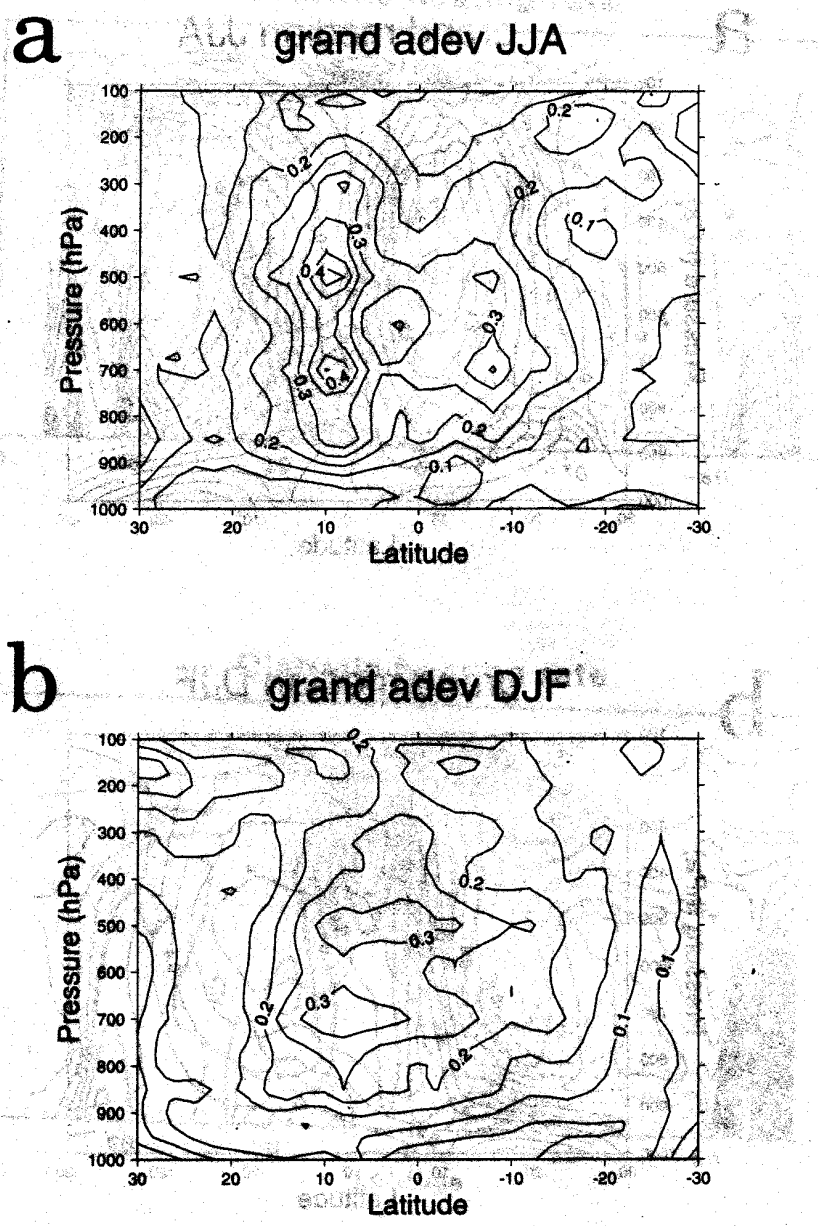

Figure 3. (a) The mean absolute deviation from the 29 model median diabatic heating rate for all the models for JJA. Contour interval is 0.1 deg C per day.
b) As in (a) except for the season DJF

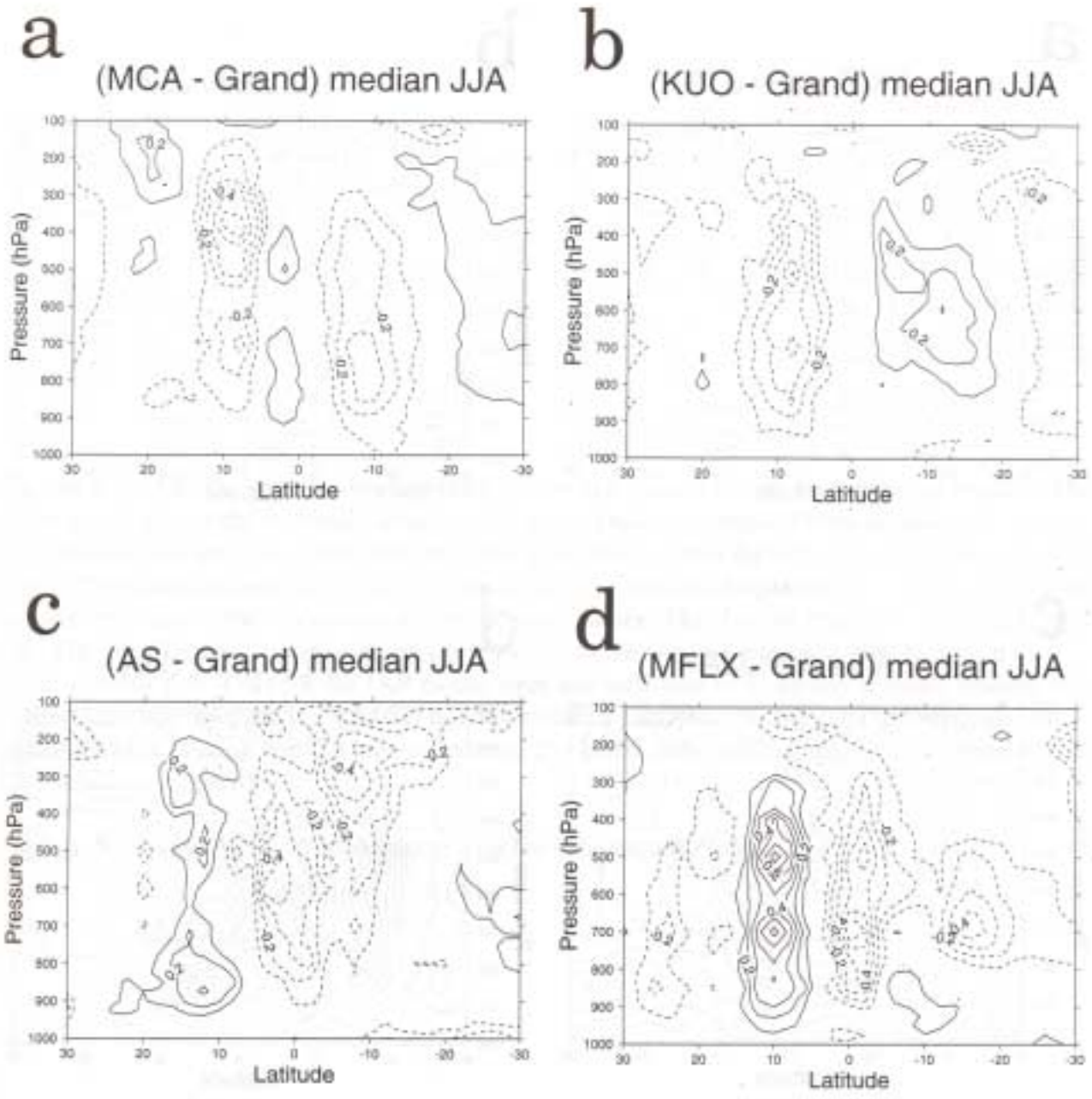

Figure 4. (a) The median diabatic heating rate computed from the models using a moist convective adjustment (MCA) scheme for JJA.
(b) As in (a) except for the Kuo (KUO) scheme.
(c) As in (a) except for the Arakawa-Schubert scheme (AS).
(d) As in (a) except for the mass-flux schemes (MFLX).
Models used in each classification are listed in Table 3.

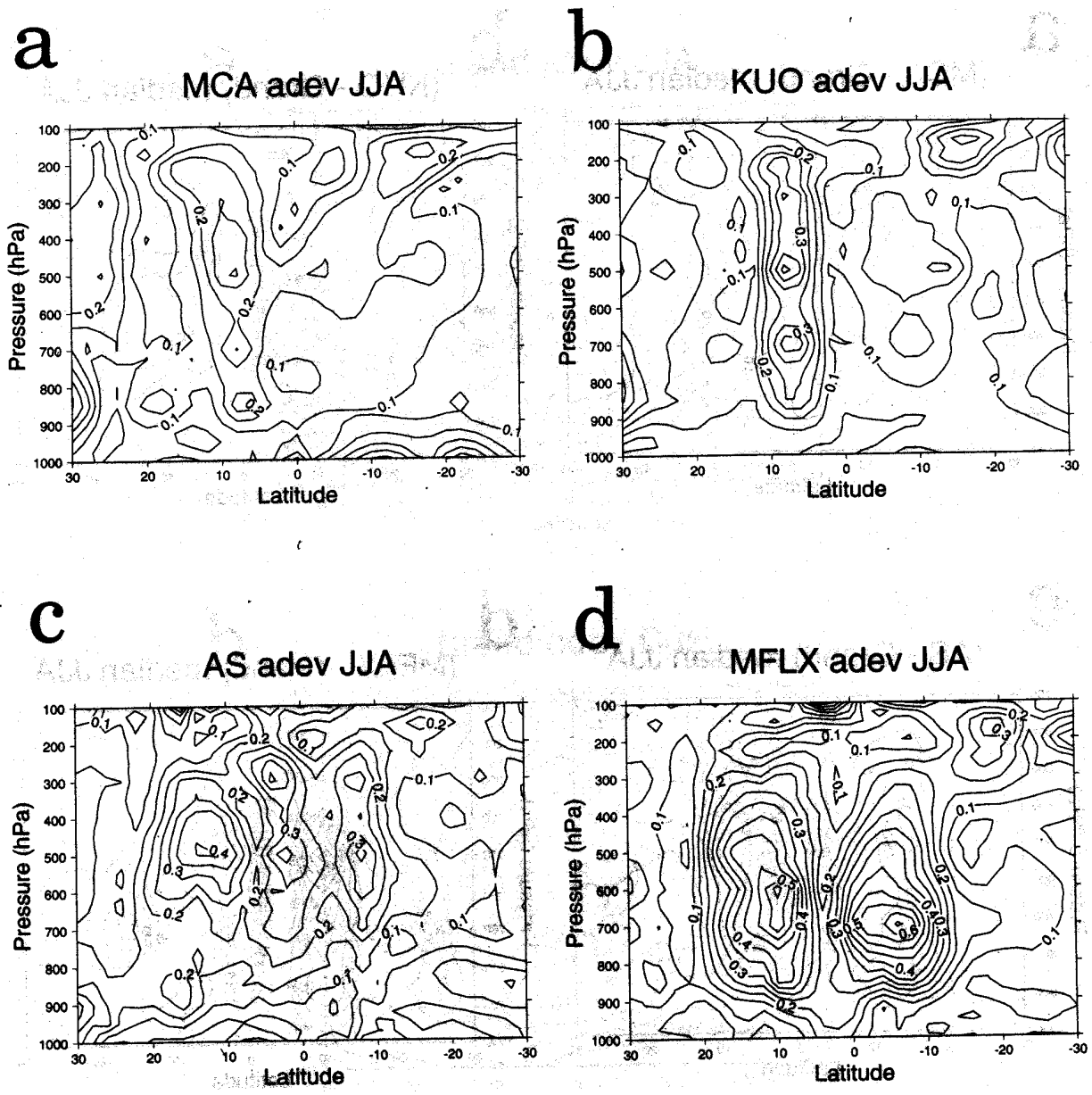

Figure 5. (a) The mean absolute deviation from the median diabatic heating rate for models using a moist convective adjustment (MCA) scheme for the JJA.
(b) As in (a) except for the Kuo (KUO) scheme.
(c) As in (a) except for the Arakawa-Schubert scheme (AS).
(d) As in (a) except for the mass-flux schemes (MFLX).
Models used in each classification are listed in Table 3..

Figures A1 - A8. The diabatic heating rates for the JJA season for all the individual models. The upper graph shows the vertically integrated diabatic heating computed from equation (2) in the text (dotted line) and from vertically integrating the results from the equation (1) in the text(solid line). The lower contour plot in each frame depicts the results of equation (1). The solid contours are positive values, the dash contours are negative values. Ths contour interval is 0.2 deg C per day. The solid line in the upper graph corresponds to the vertical integral of the values in the lower contour plot. Data for the IAP model were not sufficient to make any diabatic heating estimates. The data from the RPN model did not included precipitation and thus the vertically integrated diabatic heating could not be estimated. The LMD indicated that there was a problem with the zonally averaged data.

Figures A9 - A16. As in A1 to A8 except for the DJF season.

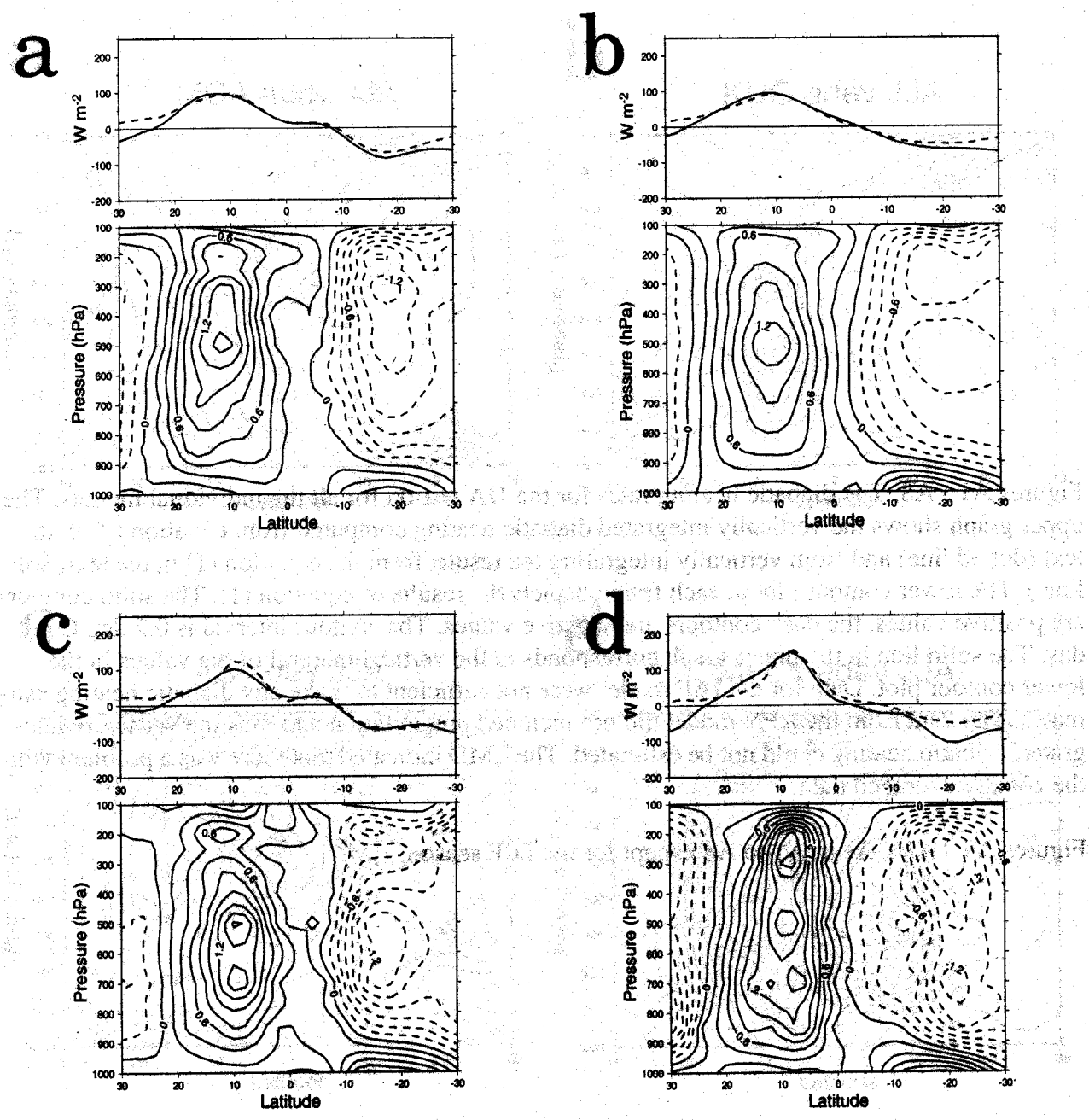

Figure A1. (a) BMRC, (b) CCC, (c) CNRM, (d) COLA.

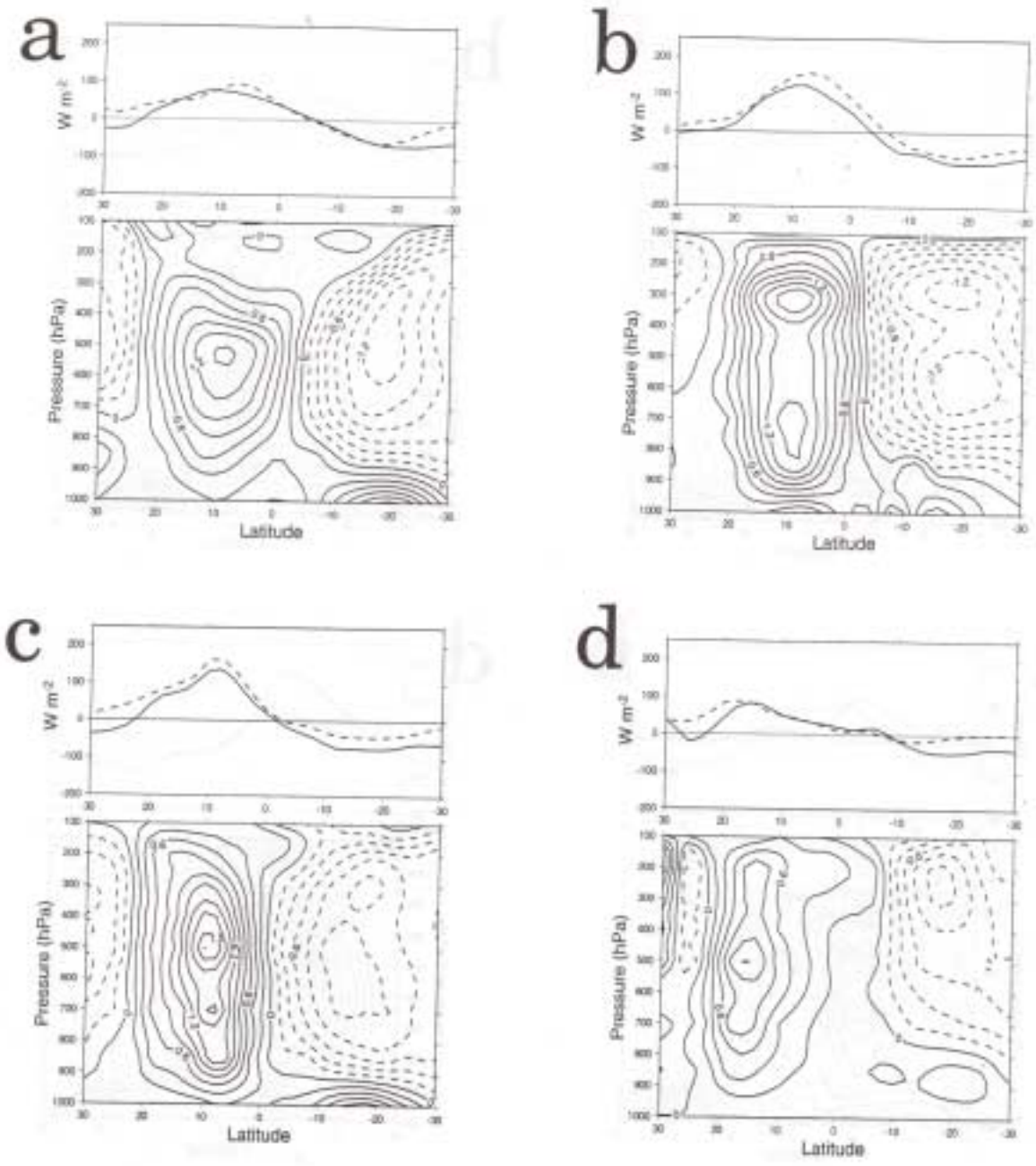

Figure A2. (a) CSIRO, (b) CSU, (c) DERF, (d) DNM

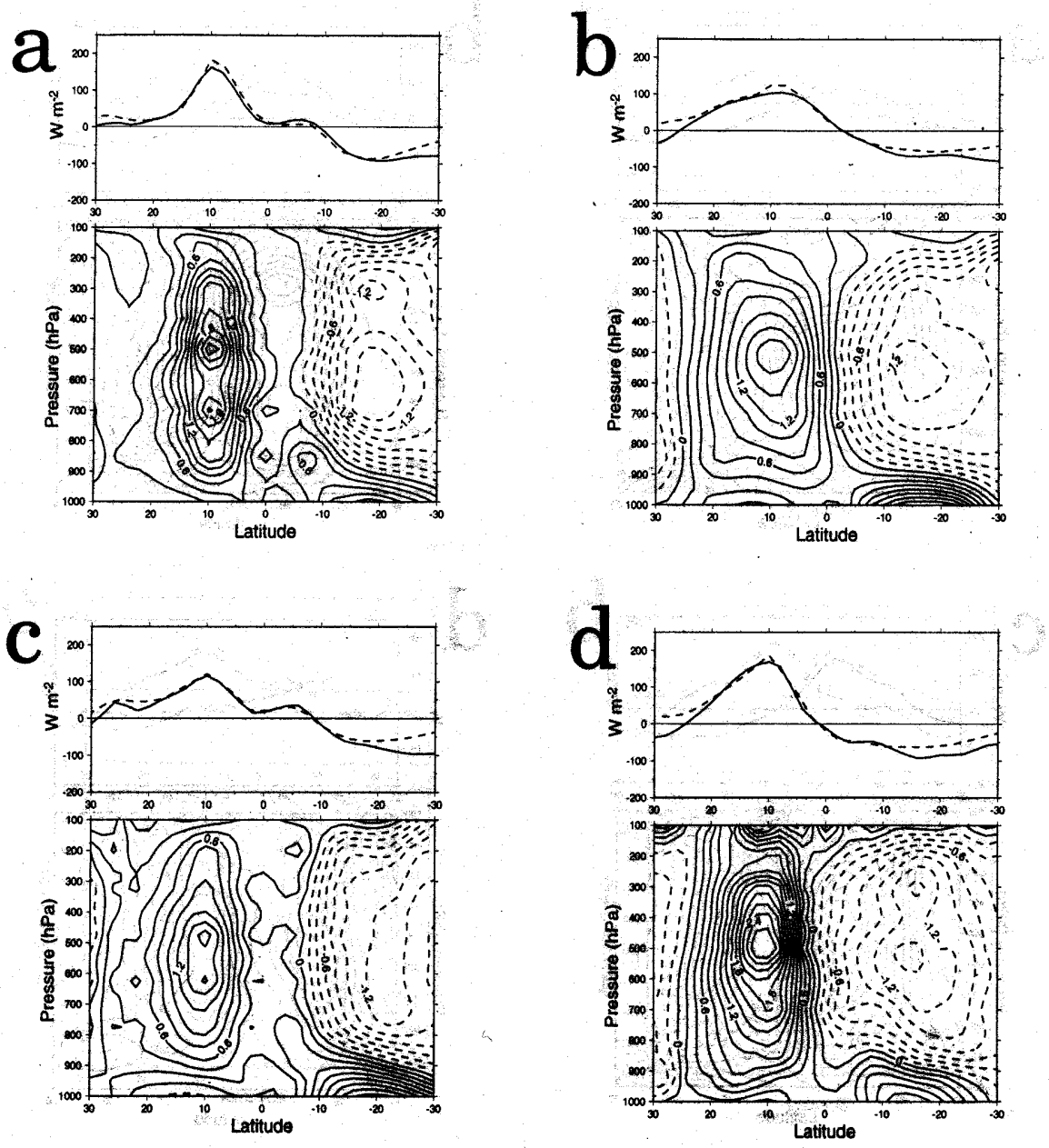

Figure A3. (a) ECMWF, (b) GFDL, (c) GISS, (d) GLA.

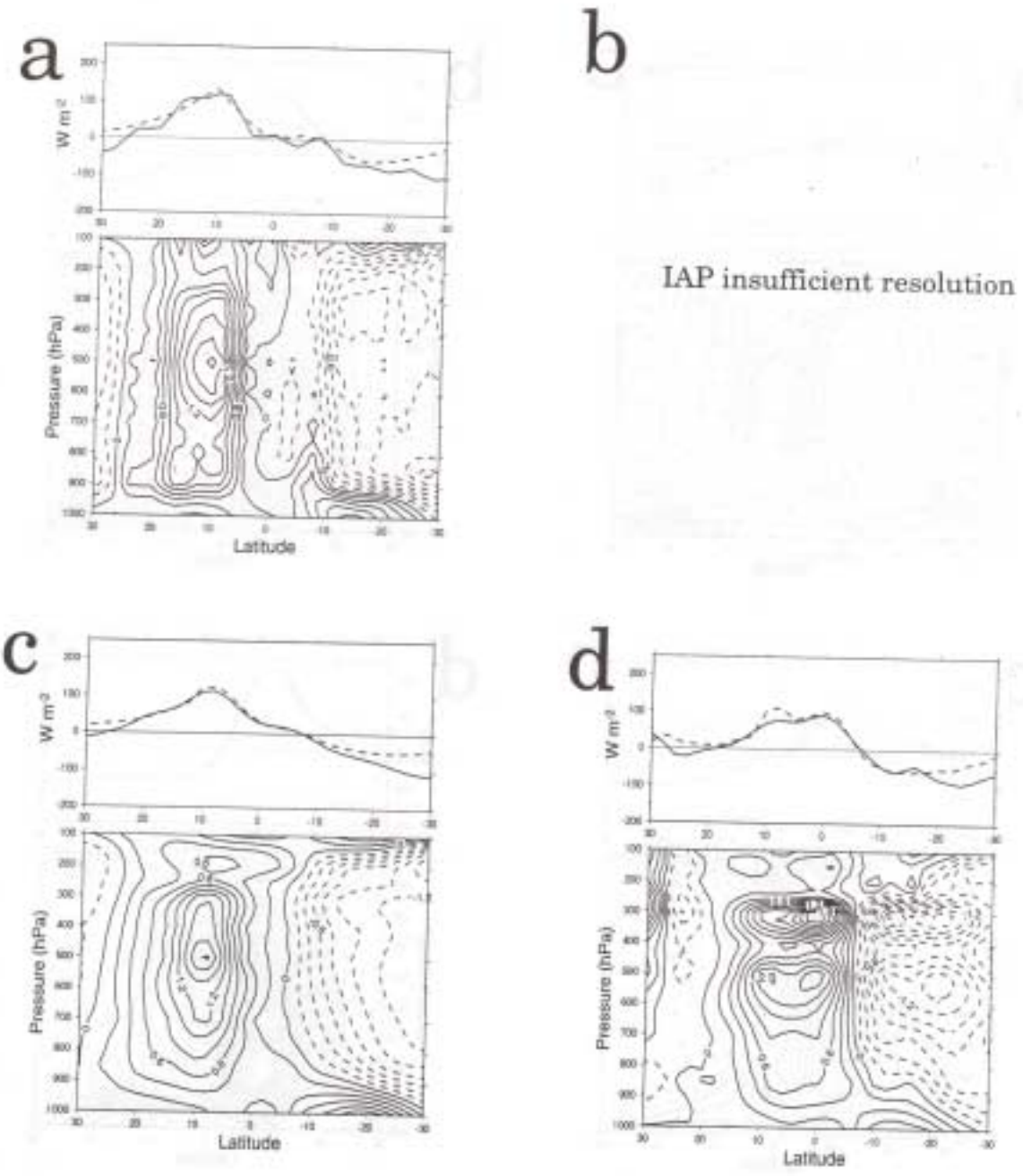

Figure A4. (a) GSFC, (b) IAP, (c) JMA, (d) LMD.

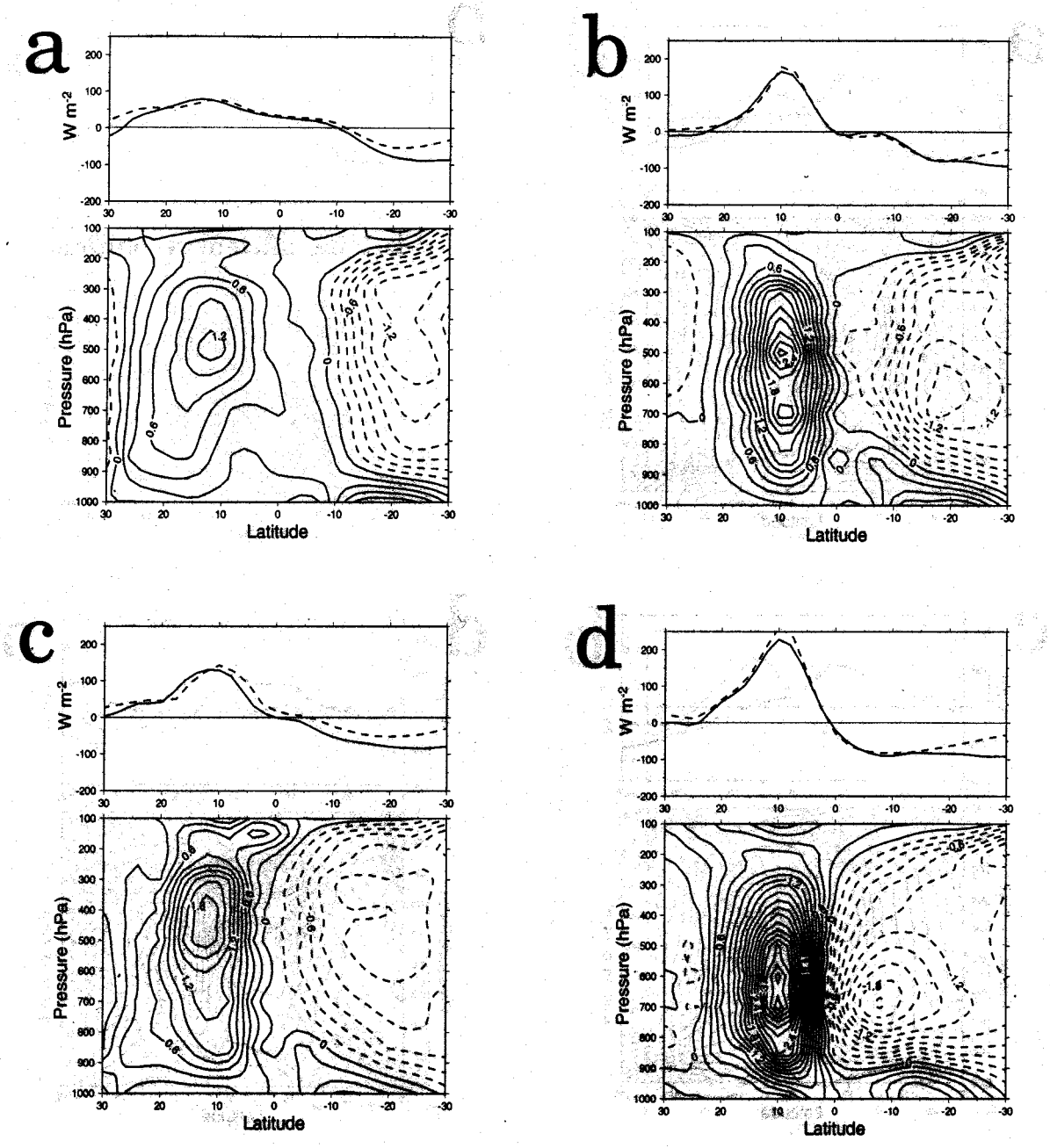

Figure A5. (a) MGO, (b) MPI, (c) MRI, (d) NCAR

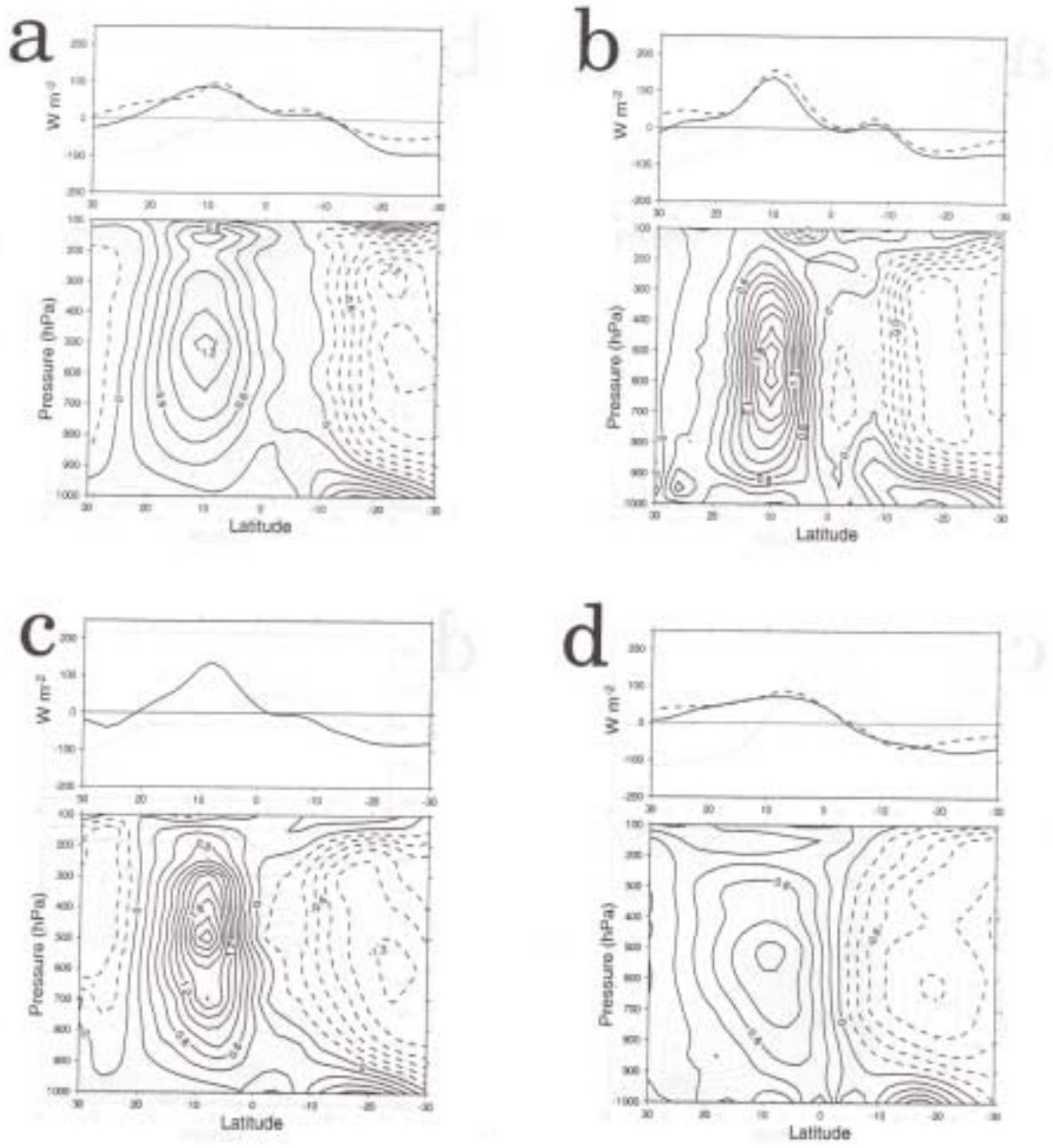

Figure A6. (a) NMC, (b) NRL, (c) RPN, (d) SUNYA.

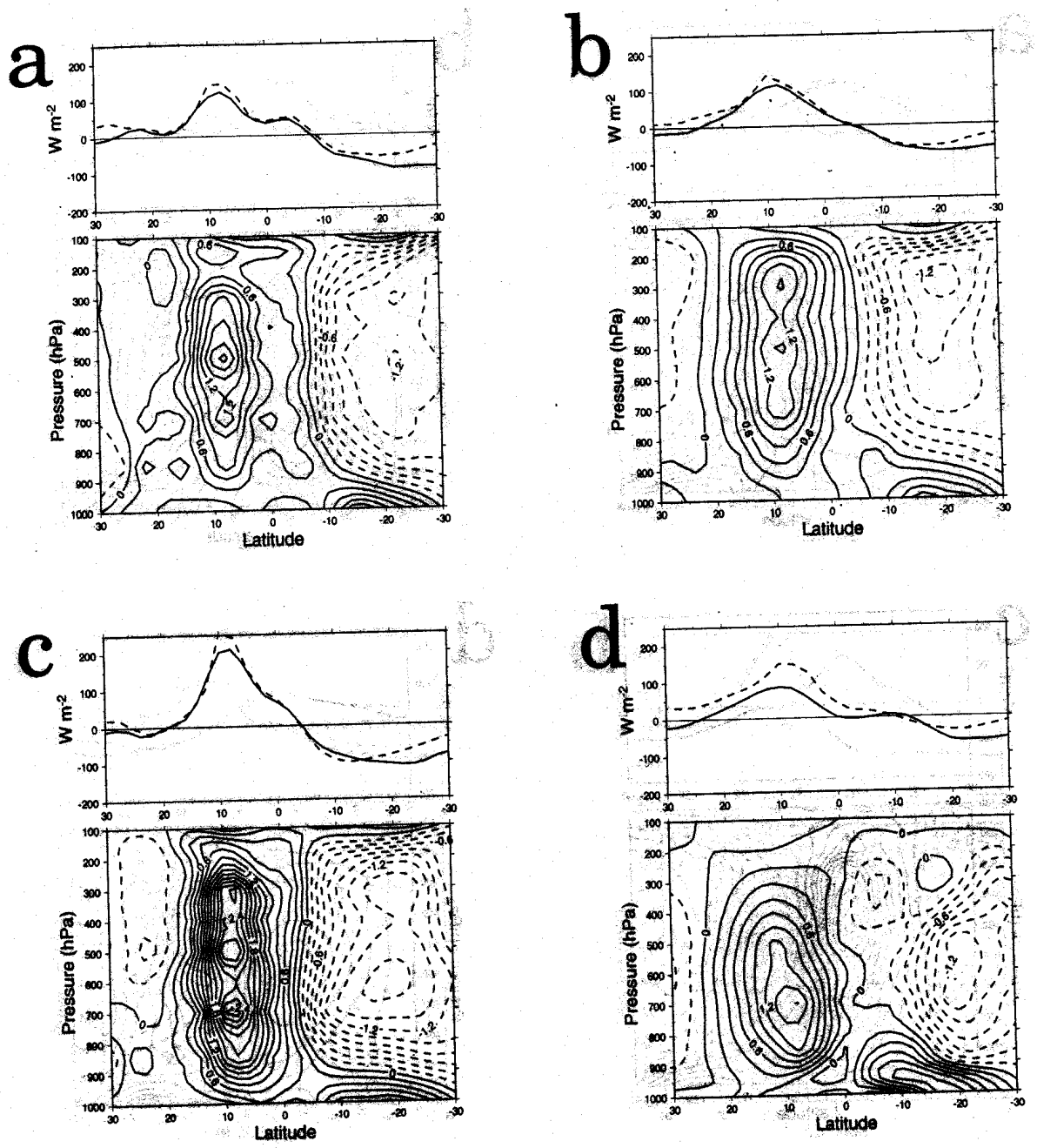

Figure A7. (a) SUNYA/NCAR, (b) UCLA, (c) UGAMP, (d) UIU.

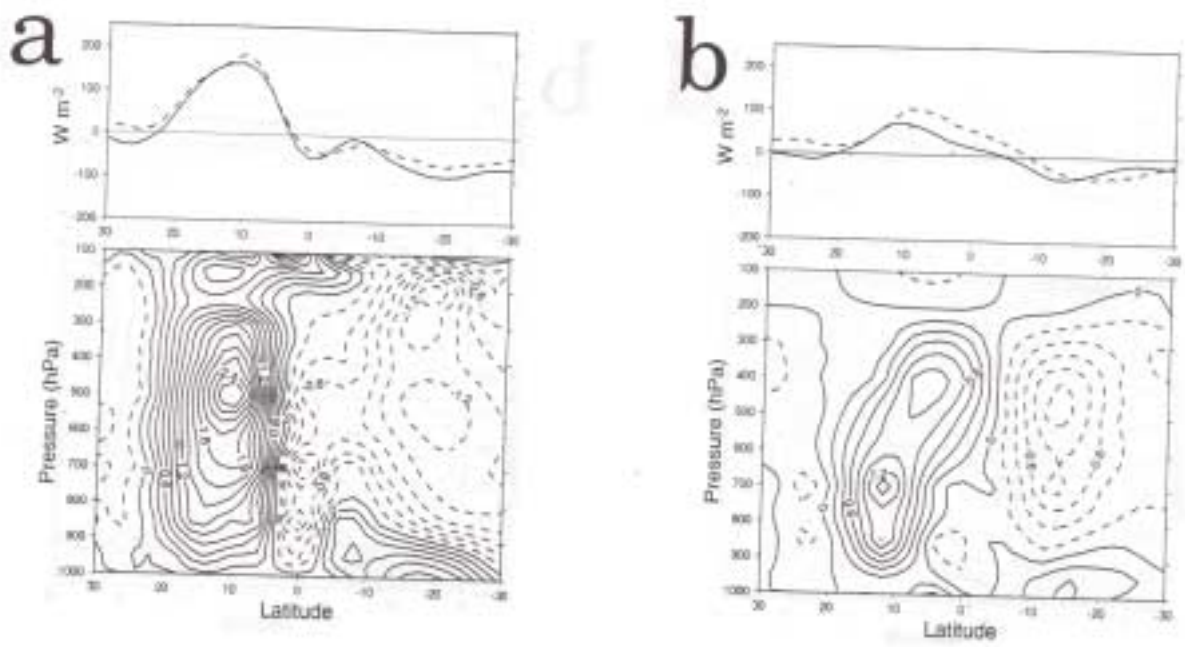

Figure A8 (a) UKMO, (b) YONU.

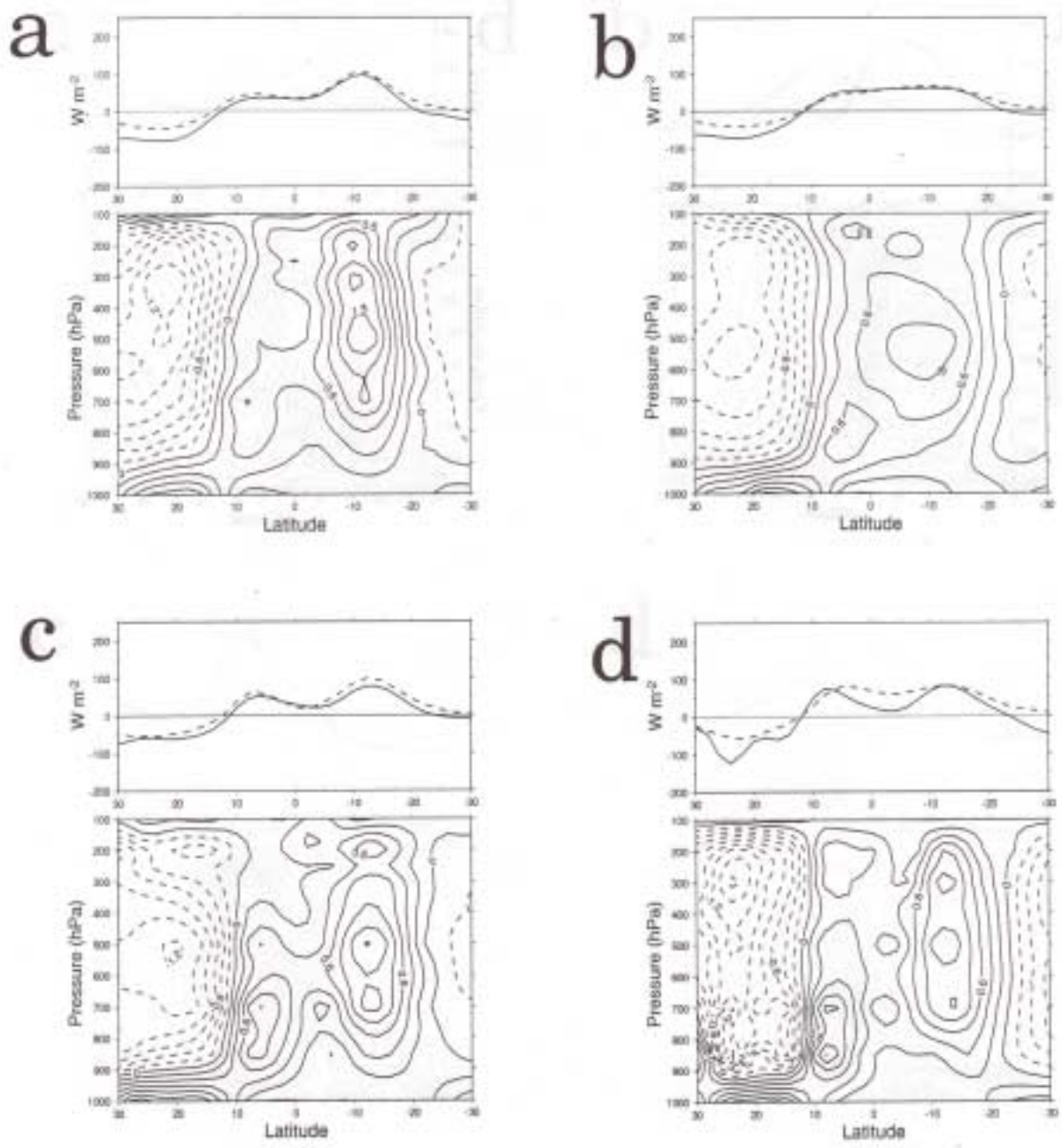

Figure A9. (a) BMRC, (b) CCC, (c) CNRM, (d) COLA.

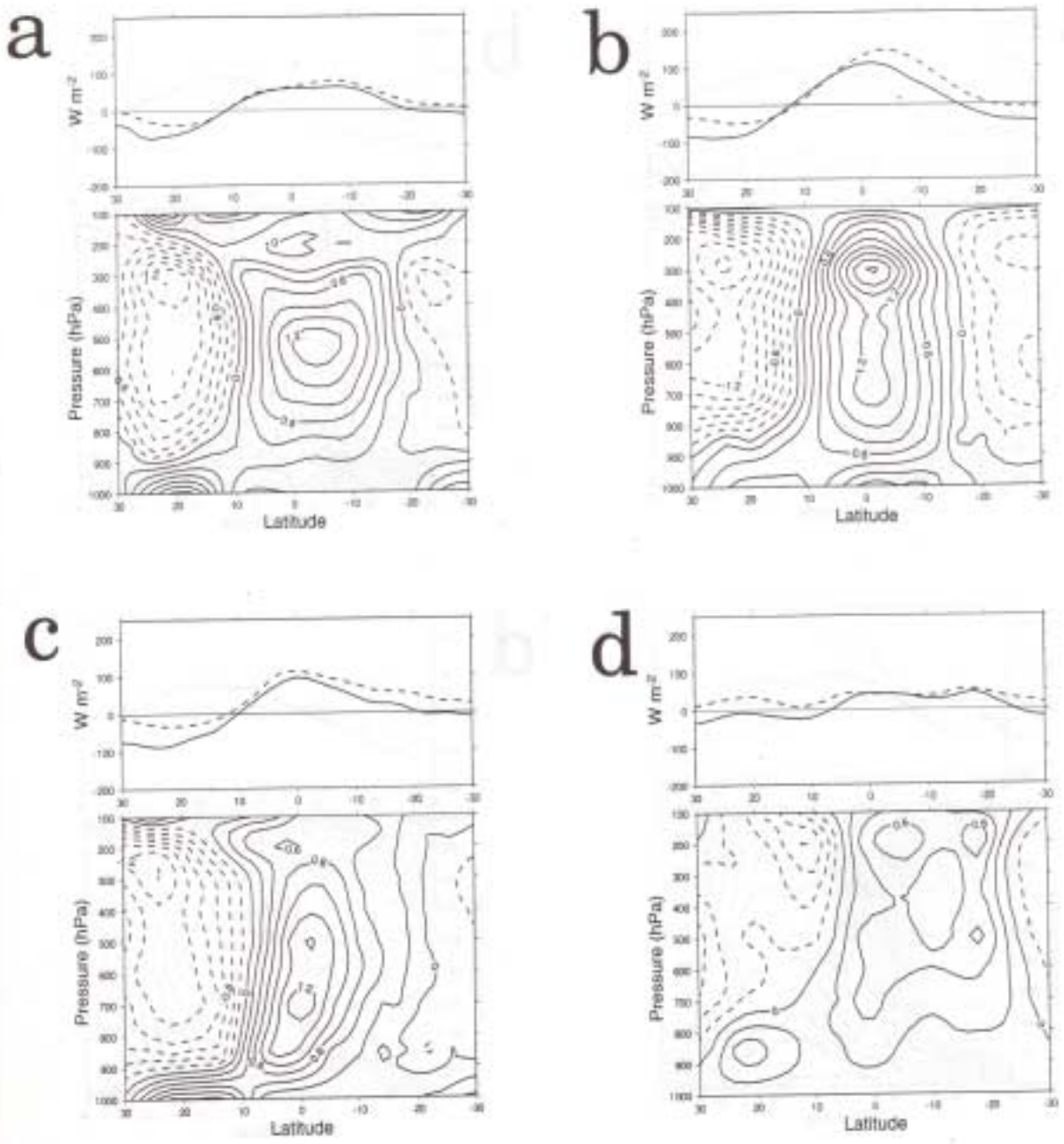

Figure A10. (a) CSIRO, (b) CSU, (c) DERF, (d) DNM.

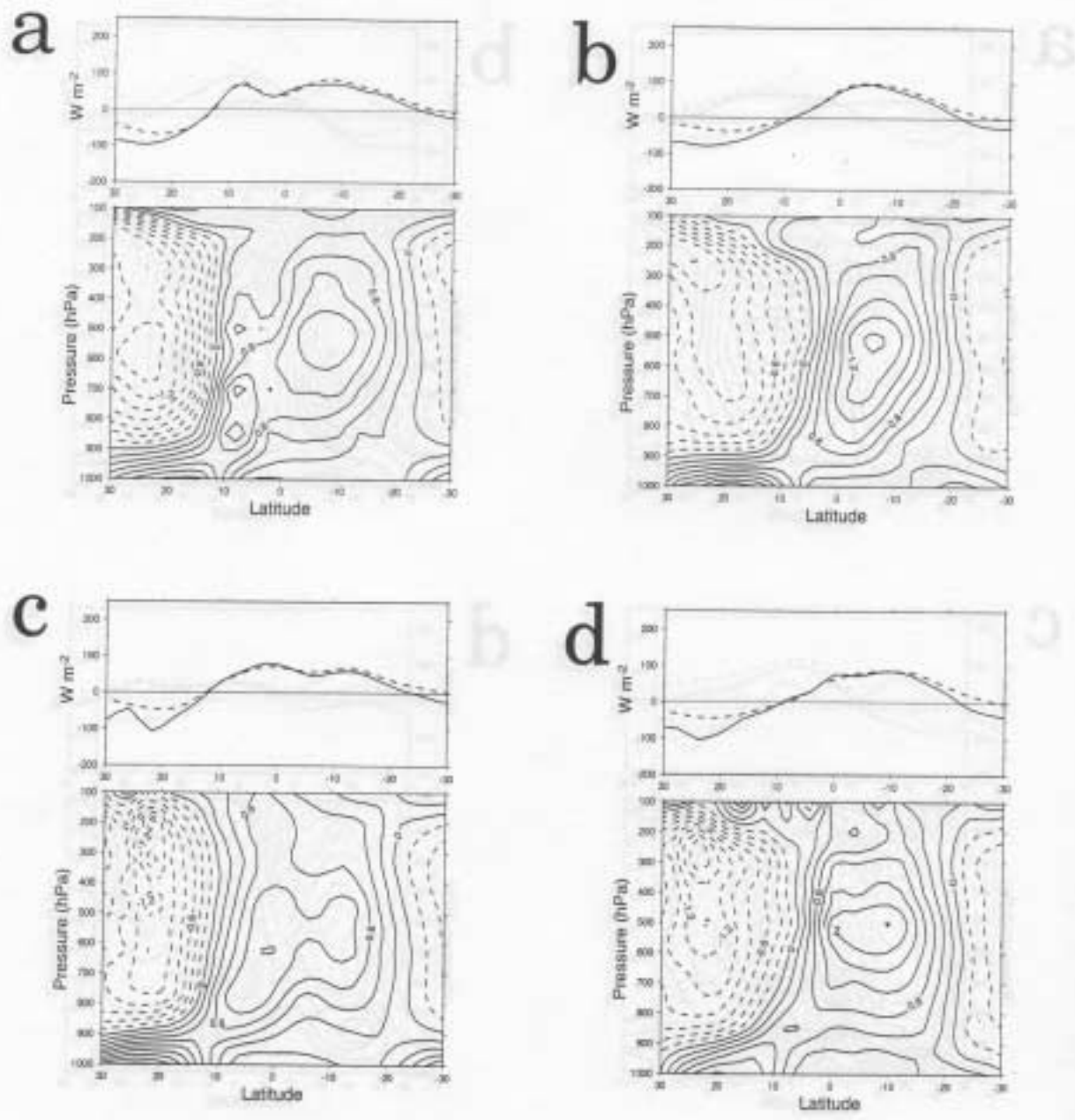

Figure A11. (a) ECMWF, (b) GFDL, (c) GISS, (d) GLA.

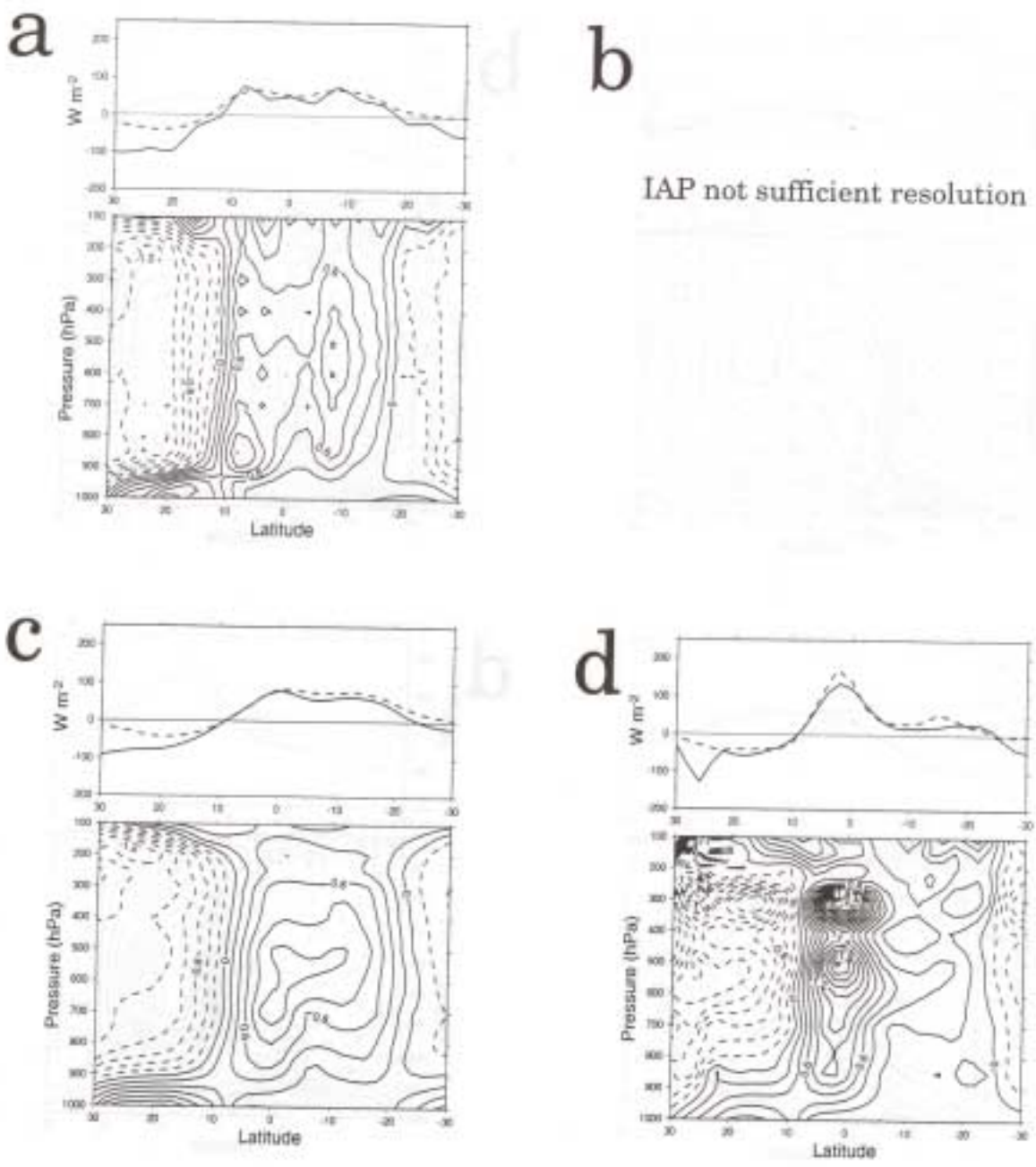

Figure A12. (a) GSFC, (b) IAP, (c) JMA, (d) LMD.

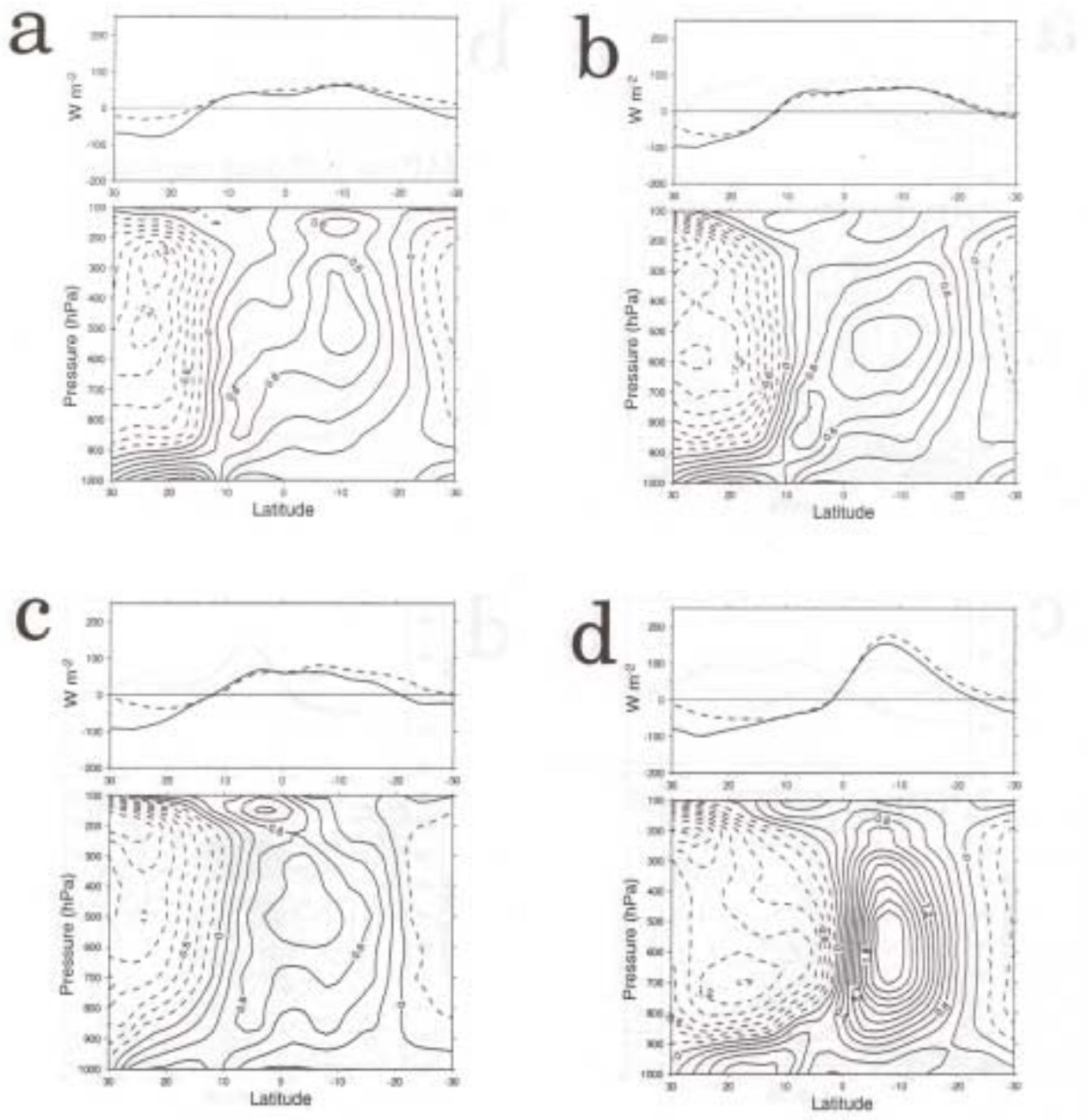

Figure A13. (a) MGO, (b) MPI, (c) MRI, (d) NCAR.

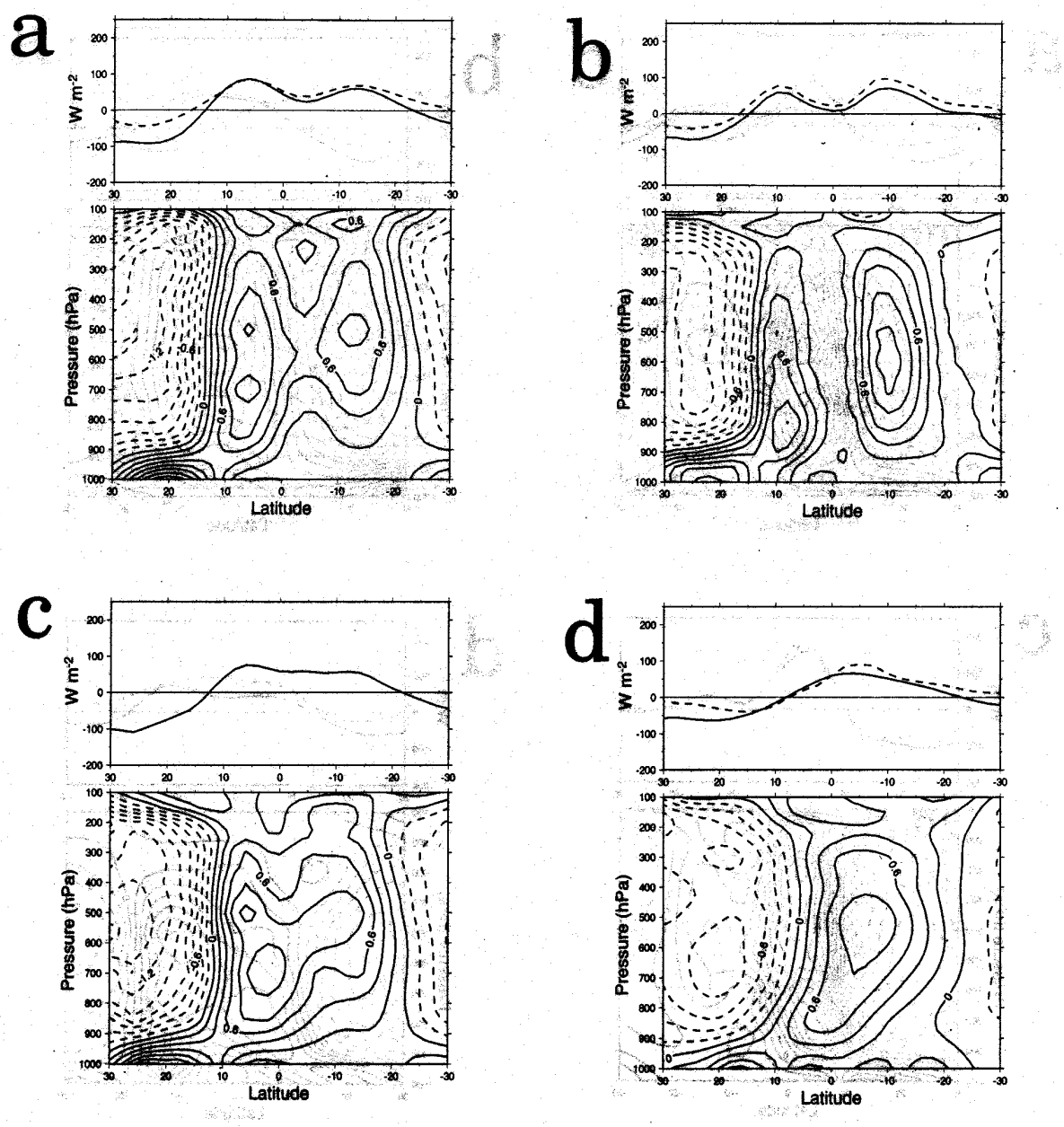

Figure A14. (a) NMC, (b) NRL, (c) RPN, (d) SUNYA

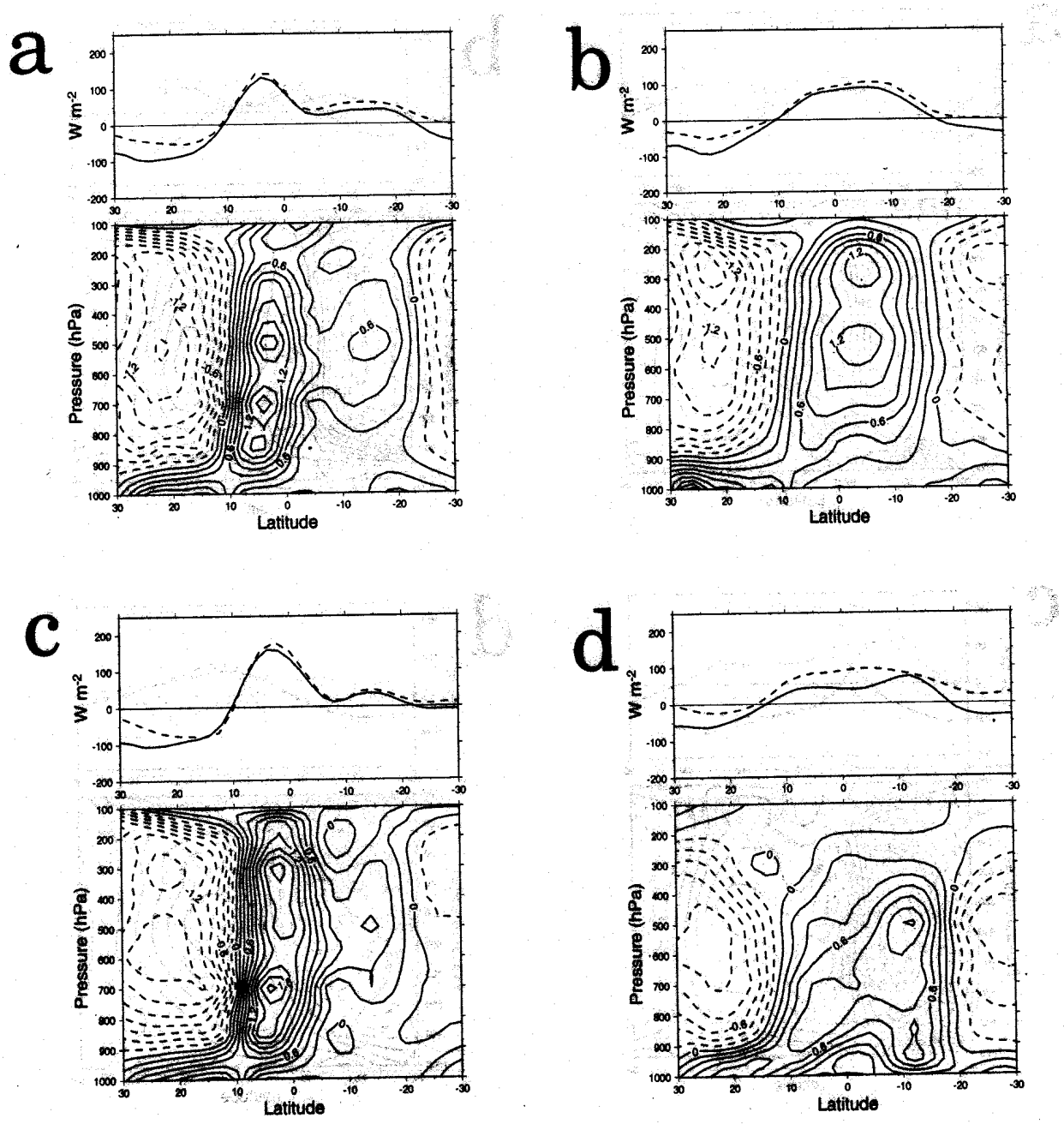

Figure A15. (a) SUNYA/NCAR, (b) UCLA, (c) UGAMP, (d) UIU.

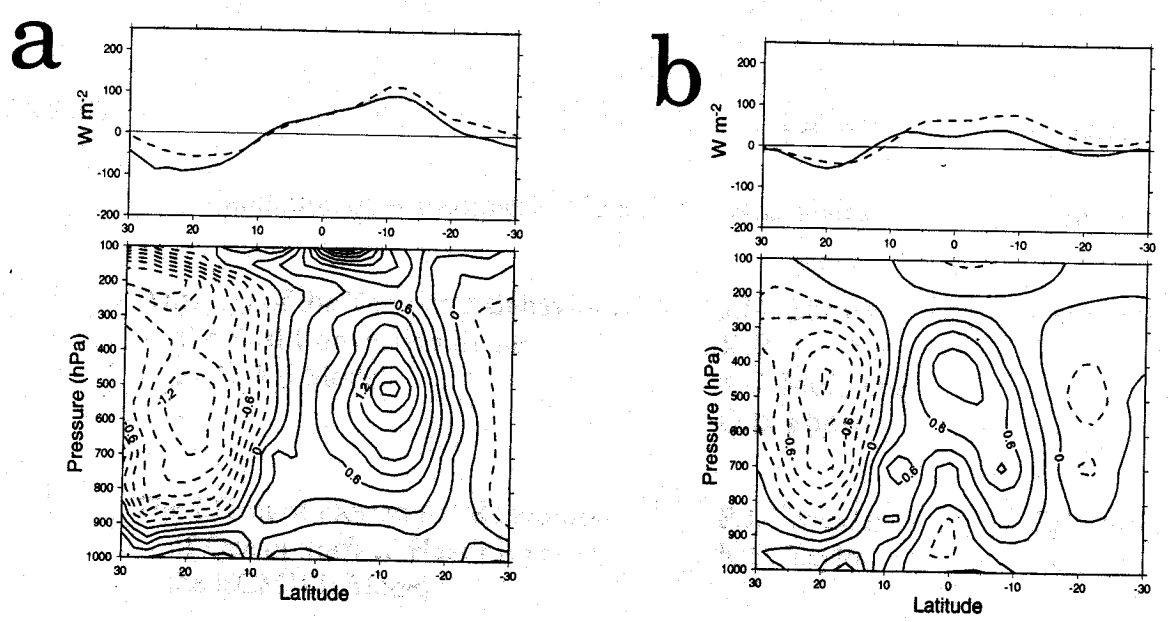

Figure A16. (a) UKMO, (b) YONU.